International Journal of Nanomedicine

Dovepress
Taylor & Francis Group

Open Access Full Text Article

ORIGINAL RESEARCH

Viral Mimetic Bacterial Outer Membrane Vesicles for Targeting Angiotensin-Converting Enzyme 2

Gna Ahn[1,2,*], Hyo-Won Yoon[1,*], Ju Hwan Jeong[3,4,*], Yang-Hoon Kim[1,*], Woo-Ri Shin[1,5,6], Min-Suk Song[3], Ji-Young Ahn[1]

[1]Department of Microbiology, Chungbuk National University, Cheongju, Republic of Korea; [2]Center for Ecology and Environmental Toxicology, Chungbuk National University, Cheongju, Republic of Korea; [3]Department of Microbiology, College of Medicine and Medical Research Institute, Chungbuk National University, Cheongju, Republic of Korea; [4]Functional Biomaterial Research Center, Korea Research Institute of Bioscience and Biotechnology, Jeongeup, Republic of Korea; [5]Department of Bioengineering, University of Pennsylvania, Philadelphia, PA, USA; [6]Department of Animal Bioscience & Integrated Biotechnology, Gyeongsang National University, Jinju, Republic of Korea

*These authors contributed equally to this work

Correspondence: Ji-Young Ahn; Min-Suk Song, Tel +82-43-261-2301; +82-43-261-3778, Email jyahn@chungbuk.ac.kr; songminsuk@chungbuk.ac.kr

Purpose: Outer membrane vesicles (OMVs) derived from Gram-negative bacteria naturally serve as a heterologous nano-engineering platform, functioning as effective multi-use nanovesicles for diagnostics, vaccines, and treatments against pathogens. To apply refined OMVs for human theranostic applications, we developed naturally exposed receptor-binding domain (RBD) OMVs grafted with antigen 43 as a minimal modular system targeting angiotensin-converting enzyme 2 (ACE2).

Methods: We constructed *E. coli*-derived OMVs using the antigen 43 autotransporter system to display RBD referred to as viral mimetic Ag43β700_RBD OMVs. Based on this, Ag43β700_RBD protein were expressed onto *Escherichia coli* (*E. coli*) membrane. Artificial viral mimetic Ag43β700_RBD OMVs were fabricated by self-assembly through membrane disruption of the Ag43β700_RBD *E. coli* using a chemical detergent mainly containing lysozyme. Through serial centrifugation to purify fabricated OMVs, spherical Ag43β700_RBD OMVs with an average diameter of 218 nm were obtained. The confirmation of the RBD expressed on OMVs was performed using trypsin treatment.

Results: Our viral mimetic Ag43β700_RBD OMVs had an impact on the theranostic studies: (i) angiotensin-converting enzyme 2 blockade assay, (ii) enzyme-linked immunosorbent assay for the OMVs, and (iii) intracellular uptake and neutralization assay. As serodiagnostic surrogates, Ag43β700_RBD OMVs were applied to ACE2 blockade and OMVs-ELISA assay to quantify neutralization antibodies (nAbs). They reduced the robust immune response in vitro, especially IL-6 and IL-1β. Experiments in mice, Ag43β700_RBD OMVs was successfully proven to be safe and effective; they produced a detectable level of nAbs with 39–58% neutralisation and reduced viral titres in the lungs and brain without weight loss.

Conclusion: The developed viral mimetic Ag43β700_RBD OMVs may therefore be applied as a nanovesicle-theranostic platform for further emerging infectious disease-related diagnosis, vaccination, and treatment.

Keywords: outer membrane vesicle, antigen 43 autotransporters, targeted delivery vehicle, theranostics, angiotensin-converting enzyme 2

Introduction

Extracellular vesicles (EVs) are spherical nanoparticles secreted by all biological systems, and in Gram-negative bacteria such as *Escherichia coli* (*E. coli*), they are specifically referred to as outer membrane vesicles (OMVs). They are formed by the bulging and pinching off of a portion of the outer membrane (OM) and consequently contain biologically active components.[1] Recently, OMVs have been exploited as diagnostic materials, immune boosters, vaccines, drug delivery, surrogate neutralisation tests, and intra- or inter-species communicators.[2–7]

E. coli-based protein engineering technologies, widely used in many biotechnological industries, have evolved to enable the production of customized proteins. The OMVs mimic heterologous expression through this bacterial engineering, owing to the

Received: 17 October 2024
Accepted: 1 January 2025
Published: 16 January 2025

Graphical Abstract

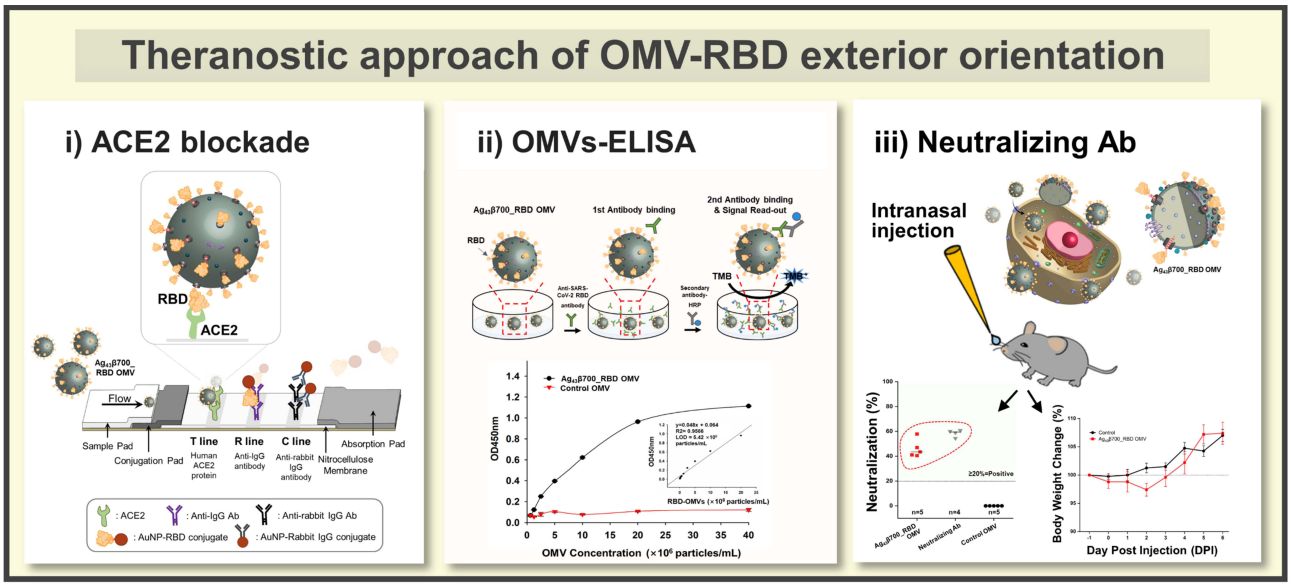

natural release mechanism of OMVs. The membranous environment of OMVs can be used to maintain the stability and exterior orientation of heterogeneous foreign antigens,[8] so that they can be used as nanovesicle-theranostic materials. Therefore, robust target protein display on the surface of OMVs may have numerous applications in combating emerging infectious diseases.[9,10]

For effective target protein display onto OMVs, we have incorporated surface display technology using antigen 43 (Ag43) of the autotransporter system of *E. coli*.[11,12] Ag43 is the simplest protein secretion-related polyprotein and consists of a signal peptide, a passenger domain, and a β-barrel domain to express the passenger domain onto the surface.[13] Original passenger and β-barrel domain includes aa 138–1039 of Ag43, but it is known that the α-helical linker domain (α-HLD; aa 700–740) within the β-barrel induces surface exposure to the outside.[11,14,15] We previously published a structural analysis of a platform capable of effective surface display using the Ag43 system with eGFP.[16] Through structural analysis, we identified that the 700–1039 amino acid sequence of Ag43 (hereafter referred to as Ag43β700) including α-HLD is the key amino acid sequence for surface exposure.

Severe acute respiratory syndrome coronavirus 2 (SARS-CoV-2) have recently emerged or re-emerged in many countries, and it still causes numerous infections.[17,18] The SARS-CoV-2 spike protein is the main key factor in the host receptor recognition for entry.[19] They decomposed into S1 and S2 proteins by protease in the body. Generally, the S1-subunit contains the receptor-binding domain (RBD) responsible for the angiotensin-converting enzyme 2 (ACE2) binding, and the S2-subunit is responsible for membrane fusion.[20,21] Based on a previous study, we constructed viral mimetic Ag43β700_RBD OMVs that the exterior orientation of OMVs was completed by replacing the passenger domain with an RBD protein, connecting it with Ag43β700. In this study, the viral mimetic Ag43β700_RBD OMVs were demonstrated to function as versatile nanovesicles for use in a SARS-CoV-2 neutralization activity test platform and as therapeutic materials, such as vaccines, by displaying the virus spike protein on the outer membrane of the OMVs, thereby enabling effective binding to the ACE2 receptor.

Our study attempted to prove that viral mimetic Ag43β700_RBD OMVs could have provided nanovesicle-theranostic platforms: ACE2 blockade, OMVs-ELISA, intracellular uptakes, and neutralizing antibodies (nAbs) production, which can be employed for emerging infectious disease diagnosis and therapeutic applications.

Materials and Methods

Ethics Statement

All animal experiments in this study were approved by the institutional animal care and use committee of Chungbuk National University, Republic of Korea (approval no. CBNUA-1977-22-02). All animal experiments were conducted

following the guidelines of the Institutional Animal Care and Use Committee (IACUC) of Chungbuk National University (approval number: CBNUA-1714-22-01) and adhered to the Guide for the Care and Use of Laboratory Animals (National Research Council, 8th edition). All experimental work, including the care and maintenance of the animals and animal housing, was carried out in a Biosafety Level Three (BSL3+) laboratory, under the recommendations and guidelines provided by the Ministry of Food and Drug Safety, Republic of Korea, and the Korea Disease Control and Prevention Agency (KCDA), Republic of Korea.

Construction of Plasmid Variants

Overall plasmid construction was based on by a previous study.[16] The Ag43 gene was amplified from the genomic DNA of *E. coli* strain K-12. SARS-CoV-2 RNA (NCCP43326) was provided by the National Culture Collection for Pathogens (NCCP, Cheongju, Republic of Korea). SARS-CoV-2 RNA was reverse transcribed using the TOPscript™ cDNA Synthesis Kit (Enzynomics, Daejeon, Republic of Korea) to amplify the SARS-CoV-2 RBD (residues Asn331–Val524) gene. The pET28b vector was modified to express the RBD–Ag43β surface display constructs with a FLAG or 6×His-tag $(GGGGS)_2$ linker, and recognition sites for restriction enzymes using the primers listed in Supplementary Table S1. The Ag43β surface display constructs and strains are summarised in Table 1.

Expression of Ag43-Fused Recombinant SARS-CoV-2 RBD

Bacterial colonies of *E. coli* strain BL21 (DE3) were transformed with the Ag43β surface display expression vector and inoculated into 5 mL Luria Bertani (LB) broth supplemented with kanamycin (50 μg/mL) and grown overnight at 37 °C with shaking at 200 rpm. The overnight cultures were inoculated into fresh LB broth supplemented with kanamycin (50 μg/mL) at a 1:100 dilution and grown to an OD_{600} of approximately 0.6. The cultures were then induced to express the Ag43β surface display proteins using isopropyl β-D-1-thiogalactopyranoside (IPTG, final concentration of 0.5 mm) at 25 °C for 20 h with shaking at 200 rpm. ClearColi BL21 (DE3) (Lucigen, Wisconsin, USA) was incubated under the same conditions as BL21 (DE3), except at a dilution ratio of 1:40 and for 24 h.

Whole-Cell Trypsin Treatment and SDS-PAGE

Whole-cell trypsin treatment was performed on the *E. coli* strain cultures until an OD_{600} of approximately 0.6 was reached, followed by centrifugation at 13,000 rpm at 4 °C for 5 min. The cell pellets were washed twice with 10 mm Tris-HCl, pH 8.0, and then resuspended in 950 μL 10 mm Tris-HCl and 50 μL trypsin (final concentration of 1 μg/mL; Sigma-Aldrich, Missouri, USA). After the incubation at 37 °C for 5 min, the cell pellets were collected by centrifugation and washed twice with 1 mL 10 mm Tris-HCl. The cell suspensions were mixed with 5× sample buffer (Biosesang, Yongin, Republic of Korea) and heated at 100 °C for 5 min. The samples were subsequently separated using SDS-PAGE at 100 V for 90 min. The relative band intensities were analysed using ImageJ software (National Institutes of Health, Maryland, USA).

Table 1 The Plasmids and Bacterial Strains Used in the Study

Plasmid	**Characteristics**	**Source**
pET28b	*Kn*^{r}	Novagen
$pAg_{43}\beta700\_RBD$	pET28b, *Ag43RBD_700* expression cassette	This work
Strain	**Genotype**	**Source**
E. coli		
DH5α	F′ Φ80*lac*Z ΔM15 Δ(*lac*ZYA-*arg*F)U169 *deo*R *rec*A1 *end*A1 *hsd*R17(rk-, mk+) *pho*A *sup*E44 *thi*-1 *gyr*A96 *rel*A1	Enzynomics
BL21 (DE3)	F– *ompT gal dcm lon hsdSB*(rB–mB–) gal λ(*DE3*)	–
ClearColi BL21 (DE3)	F– ompT hsdSB (rB- mB-) gal dcm lon λ(DE3 [lacI lacUV5-T7 gene 1 ind1 sam7 nin5]) msbA148 ΔgutQ ΔkdsD ΔlpxLΔlpxMΔpagPΔlpxP ΔeptA	Lucigen
$Ag_{43}\beta700\_RBD$	ClearColi BL21 transformed with $pAg_{43}\beta700\_RBD$	This work

https://doi.org/10.2147/IJN.S497742

Whole-Cell Trypsin Treatment and SDS-PAGE

OMVs from *E. coli* cells expressing Ag43-fused SARS-CoV-2 RBD were isolated as previously described,[22,23] with slight modifications. *E. coli* cells (OD_{600} approximately 20) were collected by centrifugation at 5000 ×g at 4 °C for 10 min and resuspended in a final volume of 36 mL Tris-HCl (200 mm, pH 8.0). Next, 2.4 mL sucrose (1 M), 2.4 mL EDTA (10 mm), 2.4 mL lysozyme (10 mg/mL), and 76.8 mL distilled water were sequentially added to the cell resuspension and incubated for 10 min at room temperature. After incubation, 1.2 mL phenylmethylsulphonyl fluoride (PMSF, 100 mm) and 240 µL aprotinin (10 mg/mL) were added to the cell suspension. The suspension was then mixed with a 120 mL extraction buffer (50 mm Tris-HCl pH 8.0 with 2% *v/v* Triton™ X-100 and 10 mm $MgCl_2$) with DNase (Sigma-Aldrich) for 25 min on ice and centrifuged at 7000 ×g for 5 min. The pelleted debris was discarded, and the supernatants were transferred to new centrifuge tubes and centrifuged at 35,000 ×g for 15 min to isolate the OM fraction. The pelleted OM fraction was washed twice and filtered through 0.45-µm filters (GE Healthcare, Illinois, USA). The isolated OMVs were resuspended in 10 mm Tris-HCl (pH 8.0) or phosphate buffered saline (PBS).

Characterisation and Trypsin Treatment of OMVs

The isolated OMVs were observed using cryo-transmission electron microscopy (cryo-TEM) on a carbon-coated copper grid. The grid-adhered OMVs were cooled using liquid nitrogen and transferred to a Tecnai G2 F20 S-TWIN TMP microscope (FEI Company, Oregon, USA) for imaging. The size and concentration of OMVs were measured using qNano Gold (Izon, Christchurch, New Zealand) with a NP 200 nanopore. Trypsin treatment of the OMVs was performed in the same manner as the whole-cell treatments. The OMVs (protein concentration 0.5 mg/mL) were treated with various trypsin concentrations (0, 0.5, 2.5, and 5 µg/mL) at 37 °C for 10 min. The reaction was stopped by mixing with 5× SDS-PAGE sample buffer and heating at 100 °C for 5 min. The samples (20 µg) were separated using SDS-PAGE and then transferred to PVDF membranes for Western blotting. Anti-SARS-CoV-2 spike rabbit antibodies (Origene, Maryland, USA) were used to detect surface expression. The washed membranes were stained with WesternBright® ECL (Advansta, California, USA), and the relative band intensities were analysed using ImageJ software.

Surface Plasmon Resonance (SPR)

The binding affinity of the ACE2 protein for the OMVs was analysed using SPR with a Biacore X-100 instrument (Cytiva, Uppsala, Sweden) at 25 °C. HBS-EP buffer (10 mm HEPES pH 7.4, 150 mm NaCl, 3 mm EDTA, and 0.005% polysorbate 20 v/v) was used as the running buffer at a flow rate of 10 µL/min. Flow cell 1 was used as a reference. To immobilise the OMVs to the CM5 sensor chip, the gold (Au) surface of the sensor chip was pre-treated with an HBS-EP buffer and activated with a 1:1 mixture of 0.05 M N-hydroxysuccinimide and 0.2 M N-ethyl-N'-(dimethylaminopropyl) carbodiimide by modifying the carboxymethyl groups of dextran. The ACE2 protein was diluted in 10 mm sodium acetate (pH 4.0) and then injected over the sensor surface to coat the surface of flow cell 2, followed by injection of 1 M ethanolamine hydrochloride (pH 8.5) to block the remaining active sites. After baseline stabilisation, different concentrations of ACE2 protein (0.1, 1, 5, 10, and 20 µM) were injected over flow cells 1 and 2 for 180 s at a flow rate of 10 µL/min and a dissociation time of 360 s. Following each experiment, the sensor chip was regenerated with 10 mm glycine (pH 2.5). Non-induced bacterial OMVs were used as controls. The SPR results were analysed using BIAevaluation software (Biacore™, Cytiva, Sweden) to determine the binding constants (K_D), as well as the association (k_{on} or ka) and dissociation (k_{off} or k_d) constants.

ACE2-Blockade LF-Strip Assay

To verify the affinity of Ag43β700_RBD OMVs for ACE2, an ACE2-blockade lateral flow (LF) assay was conducted. The ACE2-blockade LF strip was designed as previously described studies.[24] Briefly, the Au nanoparticles (AuNPs) were conjugated to rabbit immunoglobulin G (IgG) (control) or RBDs under pH 8.4. Nitrocellulose membranes were blocked with PBS and dried at 37 °C for 1 h. Human ACE2 protein (1 mg/mL) as the test (T) line, 1 mg/mL anti-IgG antibody as the reaction (R) line, and 1 mg/mL anti-rabbit IgG antibody as the control (C) line were manually spotted onto the nitrocellulose membrane. Conjugation pads were blocked with PBS containing 2% bovine serum albumin (BSA) and

dried at 37 °C for 4 h. AuNP–RBD or IgG were applied to the conjugation pad and dried at 37 °C for 1 h. After applying Ag43β700_RBD OMVs of varying concentrations onto the strip, the band intensity was quantified using ImageJ.

Enzyme-Linked Immunosorbent Assay (ELISA)

Indirect ELISAs were conducted using anti-SARS-CoV-2 RBD IgG. Ninety-six-well maxibinding immunoplates (SPL Life Sciences, Pocheon, Republic of Korea) were coated with 50 μL recombinant SARS-CoV-2 spike protein RBD (Sigma-Aldrich) or Ag43β700_RBD OMVs dilutions ranging from 0.07×10^6 to 4.00×10^7 particles/mL in PBS overnight at 4 °C. The plates were then washed three times with 200 μL 0.05% PBS-Tween (PBS-T) and blocked for 2 h at 25 °C using blocking buffer [3% (w/v) BSA in PBS-T]. The plates were washed three times and incubated with anti-SARS-CoV-2 S rabbit IgG (diluted 1:1000 in blocking buffer) for 2 h at 25 °C. After washing, 50 μL secondary horseradish peroxidase-conjugated anti-rabbit IgG (diluted 1:10,000 in blocking buffer) was added to the wells and incubated for 2 h at 25 °C. The plates were then washed and 100 μL 3.3′,5,5′-tetramethylbenzidine (TMB) substrate solution (Thermo Scientific, USA) was added to each well and incubated for 30 min. The reaction was stopped with 100 μL 0.16 M sulphuric acid, and the absorbance of each well was measured at 450 nm using a microplate reader (SpectraMax M2e, Molecular Devices, California, USA).

Confocal Fluorescence Microscopy of OMV Uptake by Vero E6 Cells

Vero E6 cells (African green monkey kidney cells, ATCC®, CRL-1586™) were cultured in Dulbecco's Modified Eagle Medium (DMEM; Welgene, Gyeongsan, Republic of Korea) supplemented with 10% (*v/v*) foetal bovine serum (FBS; Gibco (USA) and 1% Antibiotic-Antimycotic (Gibco, New York, USA) at 37 °C in a 5% CO_2 incubator. Ag43β700_RBD OMVs (2.0×10^{12} particles/mL) were mixed with 1% *v/v* DiI cell-labelling solution (Invitrogen, Massachusetts, USA) and incubated at 37 °C for 30 min. To remove the residual DiI, the labelled Ag43β700_RBD OMVs were centrifuged at 35,000 ×g for 30 min. The pelleted DiI-labelled Ag43β700_RBD OMVs were then resuspended in PBS. For the cell-uptake assays, Vero E6 cells were seeded into 12-well plates (4.8×10^6 cells/well), covered with glass coverslips, and cultured overnight. Next, 50 μL Ag43β700_RBD OMVs (3.0×10^{12} particles/mL) in fresh culture medium were added to each well and incubated for 1 h at 37 °C. The attached cells were washed three times with PBS and fixed with 4% *w/v* paraformaldehyde. The cells were then washed three times with PBS and mounted in mounting medium with DAPI (VectorLab, California, USA). Images were acquired using a confocal laser scanning microscope LSM 880 (Zeiss, Oberkochen, Germany).

Time-Dependent ACE2 Recognition by OMVs in Vero E6 Cells

Cells were seeded into a 6-well plate (3×10^5 cells/well) and incubated for 24 h. OMVs (10 μg) were then added to the wells and incubated for 10, 30, 60, and 120 min. The cell culture media containing OMVs was then discarded, and the cells were washed three times with Dulbecco's PBS. The collected protein (10 μg) was separated using 10% SDS-PAGE and then subjected to Western blotting with anti-ACE2 rabbit (Abcam) and anti-actin rabbit (Invitrogen) antibodies to detect ACE2 recognition by the OMVs.

Immune Cytokine Test in Raw 264.7 Cells

Cytokine assays were performed using Raw 264.7 cells (ATCC®, TIB-71™) cultured under the same conditions and procedures as those described for Vero E6 cells. The cells were seeded into a 96-well plate (3×10^4 cells/well) and incubated for 24 h. Different concentrations of OMVs (50, 5, 0.5, and 0.05 μg/mL) and experimental controls (100 ng/mL lipopolysaccharide (LPS) and 50 μg/mL control OMVs) were then added to each well and incubated for 24 h. The cell culture media were then collected and centrifuged at 1500 ×g at 4 °C for 10 min to remove debris. Cytokines were then detected using cytokine multiplex ELISA (Arigo, Taiwan) according to the manufacturer's protocol.

Mouse Immunisation and ELISA for Viral nAbs

Eight-week-old female B6.Cg-Tg (K18-ACE2) 2Prlmn/J mice (strain no. 034860) were obtained from Jackson Laboratory (Bar Harbor, ME, USA) and housed in separate groups prior to infection. For the neutralisation test, the test group of female

C57/Bl6 mice (n = 5) was immunised intranasally with Ag43β700_RBD OMVs (8.0×10^8 particles/mouse) four times (days 0, 1, 2, and 2.5). The control group was immunised intranasally with non-induced control OMVs. The mice were observed for 6 days, and changes in body weight were recorded as an indication of morbidity. Blood samples were obtained using the retro-orbital plexus puncture method, and the collected serum was stored at −20 °C. To detect the presence of nAbs, ELISAs (Thermo Scientific) were performed according to the manufacturer's instructions. The percentage of neutralisation was calculated as:

$$\%\ of\ neutralisation = [1 - (\frac{sample\ abs}{negative\ control\ abs})] \times 100$$

where *sample abs* represents the absorbance of the tested sample and *negative control abs* represents the absorbance of the negative control provided with the kit at 450 nm.

Virus Infection in K18-hACE2 Mice and Treatment Regimen

The β-CoV/Korea/KCDC03/2020 (NCCP43326) virus was provided by the NCCP. Molnupiravir (MPV) was obtained from MedChemExpress (Monmouth Junction, NJ, USA). The MPV stock solution was prepared with a vehicle containing 1% dimethyl sulphoxide and 20% sulfobutylether-β-cyclodextrin (MedChemExpress) in 0.9% NaCl and stored at –20 °C. The experimental mice were divided into four groups, with 10 mice in each group: group 1, infection-only; group 2, MPV (20 mg/kg); group 3, control OMVs; and group 4, Ag43β700_RBD OMVs. For infection, mice were anesthetised by isoflurane inhalation and intranasally inoculated with 50 μL 5 mouse lethal dose (MLD_{50}) β-CoV/Korea/KCDC03/2020 on day 0. On the same day, MPV was administered orally. For the survival test, OMVs (control and Ag43β700_RBD OMVs) were administered intranasally 1 h before infection and 1, 24, and 48 h post-infection. After infection and treatment, the mice were carefully monitored for body weight changes and survival from days 0 to 14. The mice were sacrificed when they lost ≥25% of their body weight before infection (as measured 1 day pre-infection). The lung and brain tissues from SARS-CoV-2-infected mice were collected at 5 days post infection (DPI) (n = 5/group) to determine the viral titres and perform histopathological and immunohistochemical analyses.

Viral Titration and Histopathological and Immunohistochemical Analyses

Lung and brain tissues from the SARS-CoV-2-infected mice were collected, homogenised by bead disruption, and centrifuged at 12,000 rpm for 5 min using TissueLyser II (Qiagen, Hilden, Germany). Ten-fold serially diluted virus-containing samples were then used to infect Vero E6 cells seeded in a 96-well plate at 2×10^6 per well and cultured in a 5% CO_2 incubator at 37 °C for 4 days or until an apparent cytopathic effect was detected and visualised with 0.2% Crystal Violet staining. Viral titre was calculated and quantified according to the Reed and Muench method and expressed as $\log_{10}$ 50% tissue culture infection dose ($TCID_{50}$) per mg of tissue. For the histopathological and immunohistochemical analyses, the tissues collected at 5 DPI were fixed in 10% formalin neutralisation buffer (Sigma-Aldrich) and processed for hematoxylin and eosin (H&E) and immunohistochemical staining. A rabbit anti-SARS-CoV-2 nucleocapsid polyclonal antibody was used as the primary antibody (Sino Biologicals, China) and further processed using a Ventana DISCOVERY ULTRA (Roche, USA) system. All slides were visualised using a Pannoramic® 250 Flash III slide scanner and evaluated using CaseViewer software (3DHISTECH Ltd., Budapest, Hungary).

Statistical Analysis

All statistical analyses were performed using the GraphPad Prism 9 software (GraphPad, San Diego, CA, USA). Statistically significant differences between more than two groups were determined using one-way analysis of variance (ANOVA) followed by Tukey's multiple comparisons test. The Kaplan–Meier method was used for survival analyses, and differences were calculated using the log-rank Mantel–Cox test with multiple comparisons.

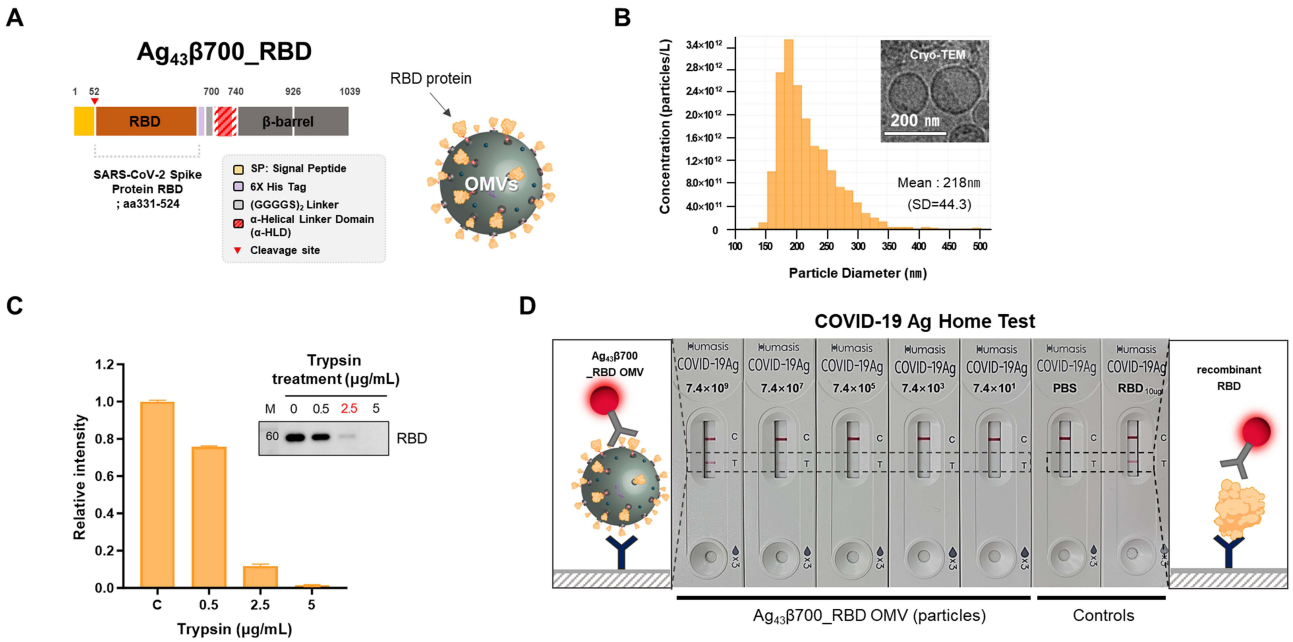

Figure 1 Construction of Ag43β700_RBD OMVs and working confirmation using commercially available COVID-19 Ag strip assay kit. (**A**) Schematic representation of the composition of *E. coli* Ag43β700_RBD (SARS-CoV spike protein RBD, amino acid residues 331–524). The SP, RBD, His-tag, glycine linker, central α-HLD, and β-barrel domain are indicated in yellow, canary, violet, grey, red, and deep grey, respectively. The insert indicates the predicted three-dimensional structure of Ag43β700_RBD on the exterior of the OMVs. (**B**) Size distribution of the Ag43β700_RBD OMVs as determined by qNano. Cryo-transmission electron microscopy (TEM) analysis was used to visually analyse the Ag43β700_ RBD OMV morphology and verify the particle size. Scale bar = 200 nm. (**C**) Extracellular trypsin treatment and Western blot analysis of Ag43β700_RBD OMVs. Significantly reduced RBD signals are seen in the Ag43β700_RBD OMVs. (**D**) Representative lateral flow (LF)-strip assay at different Ag43β700_RBD OMV concentrations. Weakly positive red test lines are visible at the "T" location of the LF-strip assay at concentrations above 7.4×10^7 Ag43β700_RBD OMVs. Purified RBDs induced a clearly visible test line. No test line is visible on the PBS/LB-strip assay. Control lines are visible at the "C" location of all the LF-strip assays.

Results

Development of OMVs with Exterior Display of Viral Spike Protein RBD

We used Ag43β autotransporter derivatives including α-HLD to generate OMVs displaying the SARS-CoV-2 spike protein RBD (Figure 1A). We analysed the morphology of the OMVs and confirmed successful exterior display of the SARS-CoV-2 spike protein RBD through trypsin treatment (Figure 1B and C) and validated their antigenicity using a SARS-CoV-2 Antigen Self-Test Kit. Representative lateral flow (LF) strip assays were used to evaluate the band intensity level for each concentration of Ag43β700_RBD-OMVs, and the positive interaction between Ag43β700_RBD-OMVs and anti-RBD antibodies was clearly visible in the T line at concentrations above 10^7 particles/mL (Figure 1D). These results indicate RBD protein was properly exposed to the outside of OMVs.

ACE2-Blockade LF-Strip Assay and Confirmation of Serodiagnostic Antigens

We tested the ability of ACE2-blockade in providing competitive advantages to early-stage virus infection with natural ACE2. Efficient display of SARS-CoV-2 RBD antigens (amino acid residues 331–524) at the surface of *E. coli* OMVs was achieved using the Ag43β700 display platform. An additional binding assay was performed using SPR to assess whether direct binding of potential therapeutics to Ag43β700_RBD OMVs can effectively block viral entry at the first infection step (Supplementary Figure S1). Various hACE2 concentrations ranging from 0.1 to 20 μM were passed through the chip surface, and Au signal changes at different OMV concentrations were recorded. hACE2 showed high binding affinity for immobilised Ag43β700_RBD OMVs with a K_D of 4.82×10^{-7} M. This finding corresponds to previous studies, which report the binding affinity of Ag43β700_RBD OMVs for hACE2 as comparable to that of the native viral RBD protein for hACE2.[25–27] The control OMVs exhibited a low binding affinity ($K_D = 1.01 \times 10^{-3}$ M). These results suggest that the displayed RBD retains its native structure, which is an important requirement for successful antigen presentation on the exterior surface of OMVs.

https://doi.org/10.2147/IJN.S497742

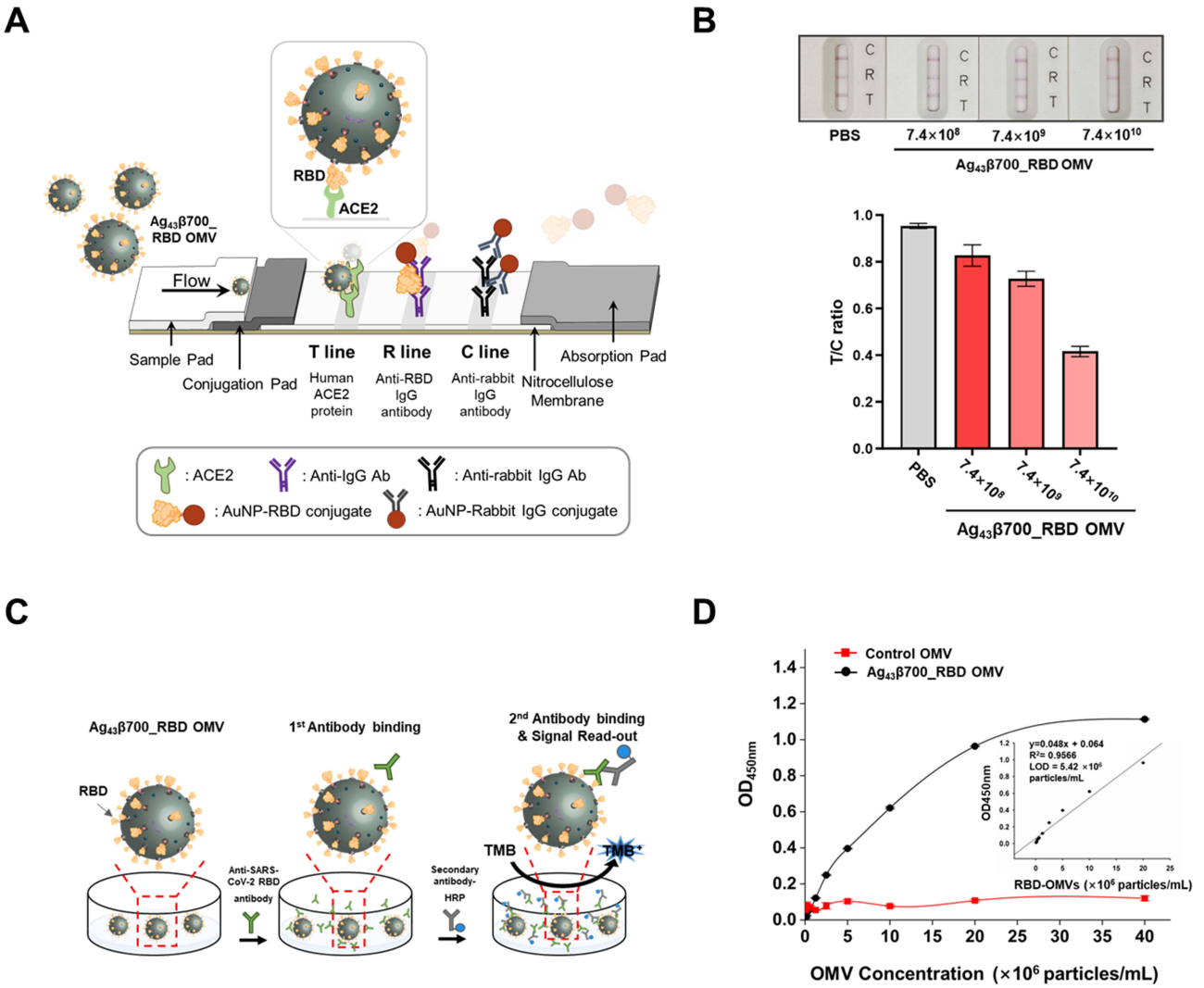

Figure 2 Neutralising ability of Ag_{43}β700_RBD OMVs and ELISA to confirm binding activity between Ag43β700_RBD OMVs and anti-SARS-CoV-2 spike RBD antibodies. (**A**) Illustration of the LF-hACE2 strip assay. Addition of phosphate buffered saline (PBS) does not block binding of the gold nanoparticle (AuNP)–RBD-conjugates to hACE2 and the RBD–ACE2 complex subsequently creates a visible test (T) line. Addition of Ag43β700_RBD OMVs can block binding of the AuNP–RBD-conjugates to hACE2, thereby decreasing the line density at the T line. The control (C) and reaction (R) lines on the LF-hACE2 strip indicate that the test ran properly. (**B**) Photos of the LF-hACE2 strip assays indicating the neutralising ability of Ag43β700_RBD OMVs using different concentrations of AuNP–RBD OMVs (upper). Signals of strips exposed to different Ag43β700_RBD OMVs concentrations were analyzed using ImageJ software (lower). (**C**) Illustration of Ag43β700_RBD OMV-based indirect ELISA platform to identify anti-SARS-CoV-2 spike RBD antibodies. Ag43β700_RBD OMVs are bound to the surface of 96-well plates. (**D**) Ag43β700_RBD OMV concentration–response curves for binding anti-RBD antibodies in the OMV-ELISA.

Subsequent analytical evaluation of hACE2 blockade using Lateral Flow (LF)-hACE2 strip assays indicated that the interaction between the RBD and hACE2 is immediately blocked by the presence of the Ag43β700_RBD OMVs (Figure 2A). The band intensity at the T line disappeared as the Ag43β700_RBD OMV concentration increased (Figure 2B). Regression analysis based on the T/C ratio confirmed that the Ag43β700_RBD OMVs inhibit the binding of the RBD to hACE2. The Ag43β700_RBD OMVs described in this study may therefore be useful for blocking viral entry into ACE2-expressing cells, thereby preventing or treating COVID-19.

In addition to the ACE2-blockade assays, we developed Ag43β700_RBD OMV-based ELISAs as a rapid and reliable tool for analysing the seroprevalence of SARS-CoV-2-specific antibodies (Figure 2C). Presentation of RBD proteins on the exterior surface of OMVs offers potential benefits over soluble RBD proteins, including unidirectional and spatially defined protein orientation, sufficient quantity, and a pseudoviral membrane environment. As shown in Figure 2D, Ag43β700_RBD OMVs were used as serodiagnostic antigens, and their performance was compared with that of recombinant viral RBD (Supplementary Figure S2). High sensitivity was exhibited with a limit of detection of 5.42 ×

10^6 particles/mL (Figure 2D). Both recombinant RBD- and OMV-based ELISAs exhibited similar binding signals across a range of antigen dilutions (RBD, 0–30.0 ng/mL; Ag43β700_RBD OMVs, 0.07–40.0 × 10^6 particles/mL). The results indicate that the Ag43β700_RBD OMV-based ELISA can determine the antibody titre in vaccinated individuals.

Intracellular Uptake of Ag43β700_RBD OMVs in vitro

We confirmed that the Ag43β700_RBD OMVs present the RBD protein on their surface, and that Ag43β700_RBD OMVs bind to ACE2, thereby providing a basis for the potential application of Ag43β700_RBD OMVs as a target-specific drug delivery vehicle for antiviral therapeutics.[28,29] To confirm in vitro ACE2 binding of Ag43β700_RBD OMVs, DiI-labelled Ag43β700_RBD OMVs were incubated with Vero E6 cells, which are ACE2 receptor-positive cells (Figure 3A).

To investigate whether ACE2-Ag43β700_RBD OMVs are involved in the regulation of ACE2 expression, we used Western blotting to examine ACE2 expression in the presence of Ag43β700_RBD OMVs. Our results indicated that ACE2 expression is upregulated following Ag43β700_RBD OMV treatment (Figures 3B and S3), which suggests that Ag43β700_RBD OMVs may regulate ACE2 at the protein level. Similar observations of ACE2 upregulation mediated by immune signalling and oxidative stress pathways have been reported in SARS-CoV-2-infected epithelial cells.[30–32] Ag43β700_RBD OMVs may therefore lead to ACE2 glycosylation and activation of downstream signal transduction,[33,34] but the characteristics of Ag43β700_RBD OMVs that induce ACE2 glycosylation require further investigation.

With respect to safety, the OMVs generated from Gram-negative bacteria may cause pyrogenicity. We subsequently assessed the levels of crucial representative pro-inflammatory cytokines in SARS-CoV-2 infection, including tumour necrosis factor alpha (TNFα), interleukin (IL)-6, and IL-1β, and found elevated pro-inflammatory cytokine expression

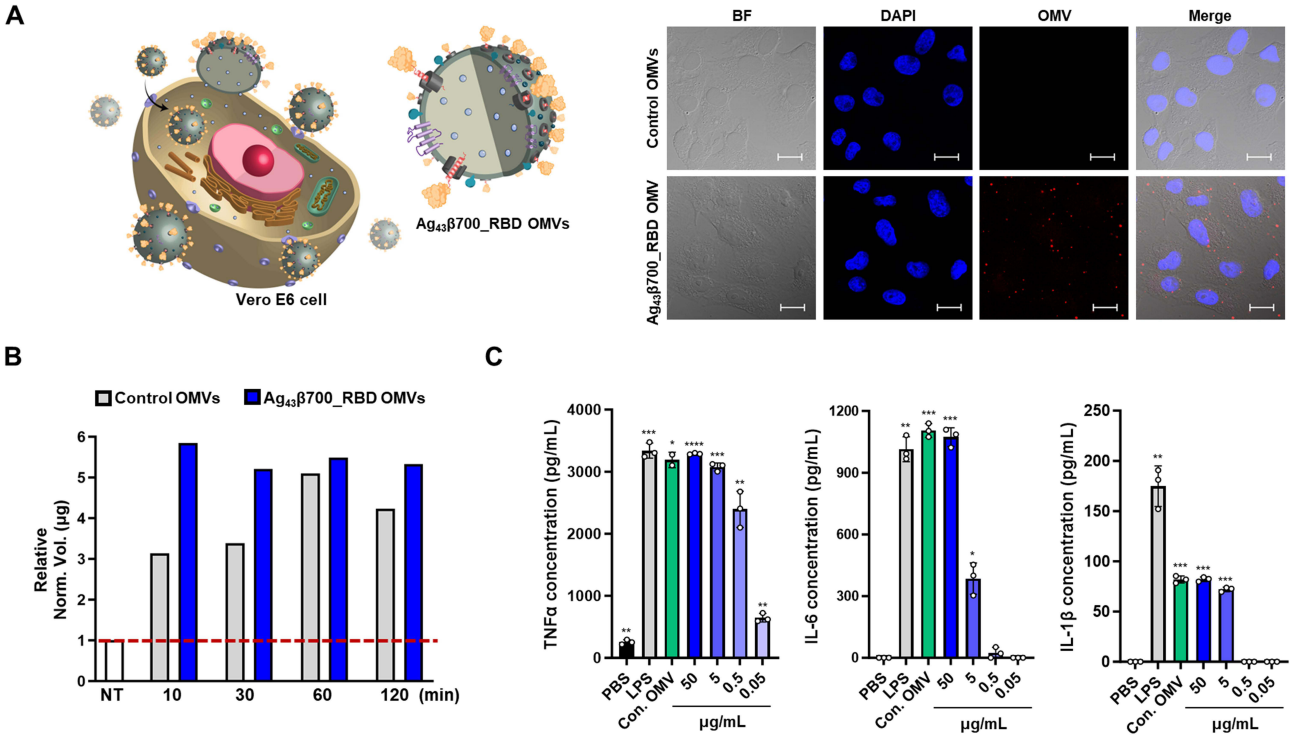

Figure 3 Intracellular uptake of Ag43β700_RBD OMVs in vitro. (**A**) Schematic illustration explain Ag43β700_RBD OMV uptake into host cells is mediated by the interaction between the viral RBD protein and the hACE receptor. Confocal fluorescence microscopy images of the binding of Vero E6 cells with DiI-labelled Ag43β700_RBD (bottom) and control (top) OMVs. Scale bar: 20 μm. (**B**) Relative ACE2 expression levels in Vero E6 cells incubated with Ag43β700_RBD OMVs for different binding times (10, 30, 60, and 120 min) determined by Western blot analysis using an anti-ACE2 antibody (see Supplementary Figure S3). The red-dotted line represents value 1 of the non-treated (NT) group. (**C**) ELISA for immune cell cytokines (TNFα, IL-6, and IL-1β). Statistical differences were analysed using an independent sample one sample *t*-test. $^{**}p = 0.0075$; $^{***}p = 0.0004$; $^{*}p = 0.0174$; $^{****}p < 0.001$; $^{***}p = 0.0001$; $^{**}p = 0.0049$ (TNFα)], [N.D; $^{**}p = 0.0012$; $^{***}p = 0.0003$; $^{***}p = 0.0006$; $^{*}p = 0.0127$; NS; N.D (IL-6)], and [N.D; $^{**}p = 0.0044$; $^{***}p = 0.0006$; $^{***}p = 0.0003$; $^{***}p = 0.0003$; N.D; N.D (IL-1β)].

https://doi.org/10.2147/IJN.S497742

levels following Ag43β700_RBD OMV treatment. As shown in Figure 3C, 100 ng/mL LPS caused a significant increase in Raw 264.7 monocytes/macrophages, but this increase was comparable to the increase seen in cells treated with a relatively high OMV concentration (50 μg/mL, 10^9 particles/mL). Moreover, the same OMV concentration did not induce cell death (data not shown), which may be attributed to Ag43β700_RBD OMVs from the LPS-mutant *E. coli* failing to exhibit specific responses with lethal toxic components, such as LPS.[35] However, it still remains unclear why IL-6 and IL-1β were rarely induced, while TNFα was highly induced.

Neutralisation Assays of Ag43β700_RBD OMVs in vivo

To further examine whether Ag43β700_RBD OMVs induce nAbs, we examined antibody titres and neutralising activity. Mice immunised with Ag43β700_RBD OMVs via intranasal inoculation at 8.0×10^8 particles/mouse on days 0, 1, 2, and 2.5 exhibited no significant decrease in body weight during 6 days of monitoring (Figure 4A). Serum samples were collected from the mice to determine the nAb levels, and the percentage neutralisation was assessed using ELISA. A cut-off of 20% was used to distinguish positive (+nAb) and negative (–nAb) samples. We found that intranasal Ag43β700_RBD OMV administration induced high serum nAb levels with 39–58% neutralisation (Figure 4B), which suggests that the use of Ag43β700_RBD OMVs as an adjuvant induces a more comprehensive immune response. Several studies have suggested that intranasal vaccination may contribute to the production of nAbs against a variety of respiratory viruses, including SARS-CoV-2.[36,37] However, there are few reports to demonstrate the necessity of adjuvants for inducing intranasal immune efficacy.[38,39] We demonstrated intranasal immunisation with Ag43β700_RBD OMVs induce nAbs, indicating that Ag43β700_RBD OMVs alone may induce both antibody- and robust cell-mediated immunity. Ag43β700_RBD OMVs may therefore have in vivo applicability in vaccine strategies to boost SARS-CoV -2 nAbs.

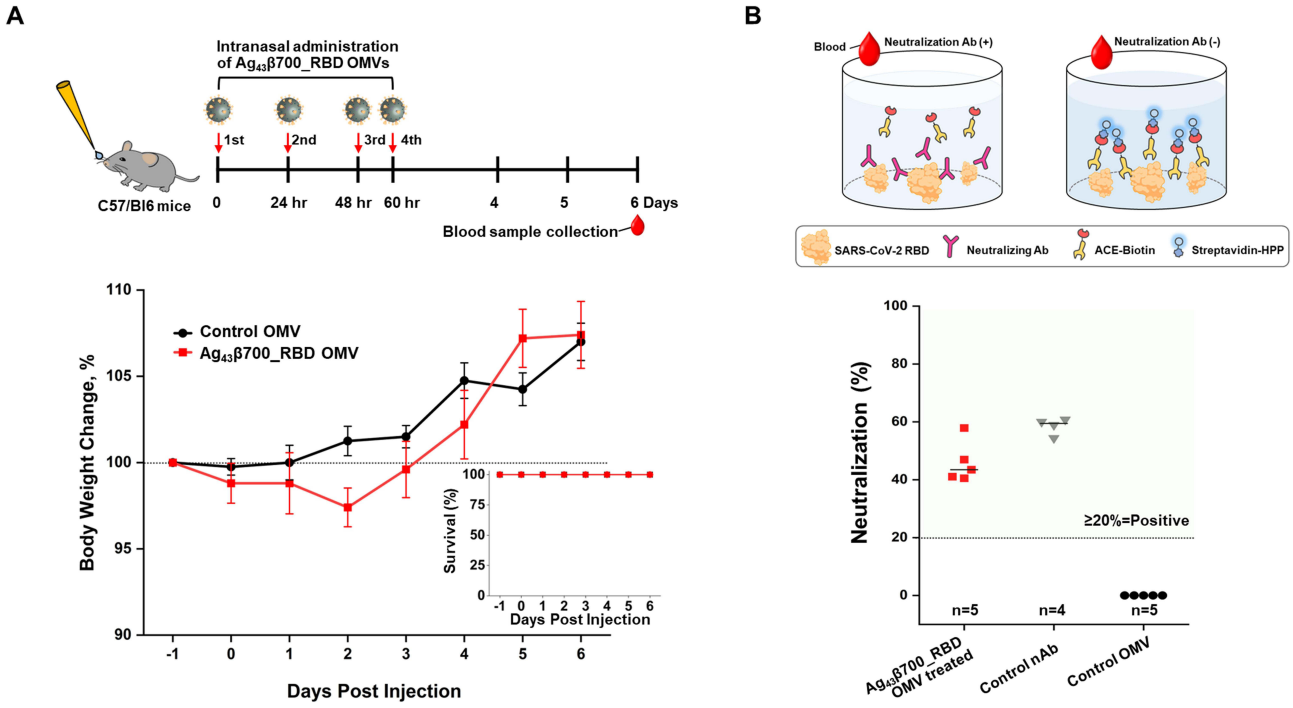

Figure 4 Neutralisation assays in vivo. (**A**) Immunisation and blood-draw schedule for C57/Bl6 mice and body weight changes (%). (**B**) Serum ELISA against SARS-CoV-2 RBD. Ag43β700_RBD OMVs improved the neutralising antibody response. The presence of neutralising sera disrupted the ACE2–RBD interaction, thus decreasing the measured signal. For commercial kits, sera presenting neutralization >20% were considered positive for the presence of neutralizing antibodies, according to the manufacturer's protocol.

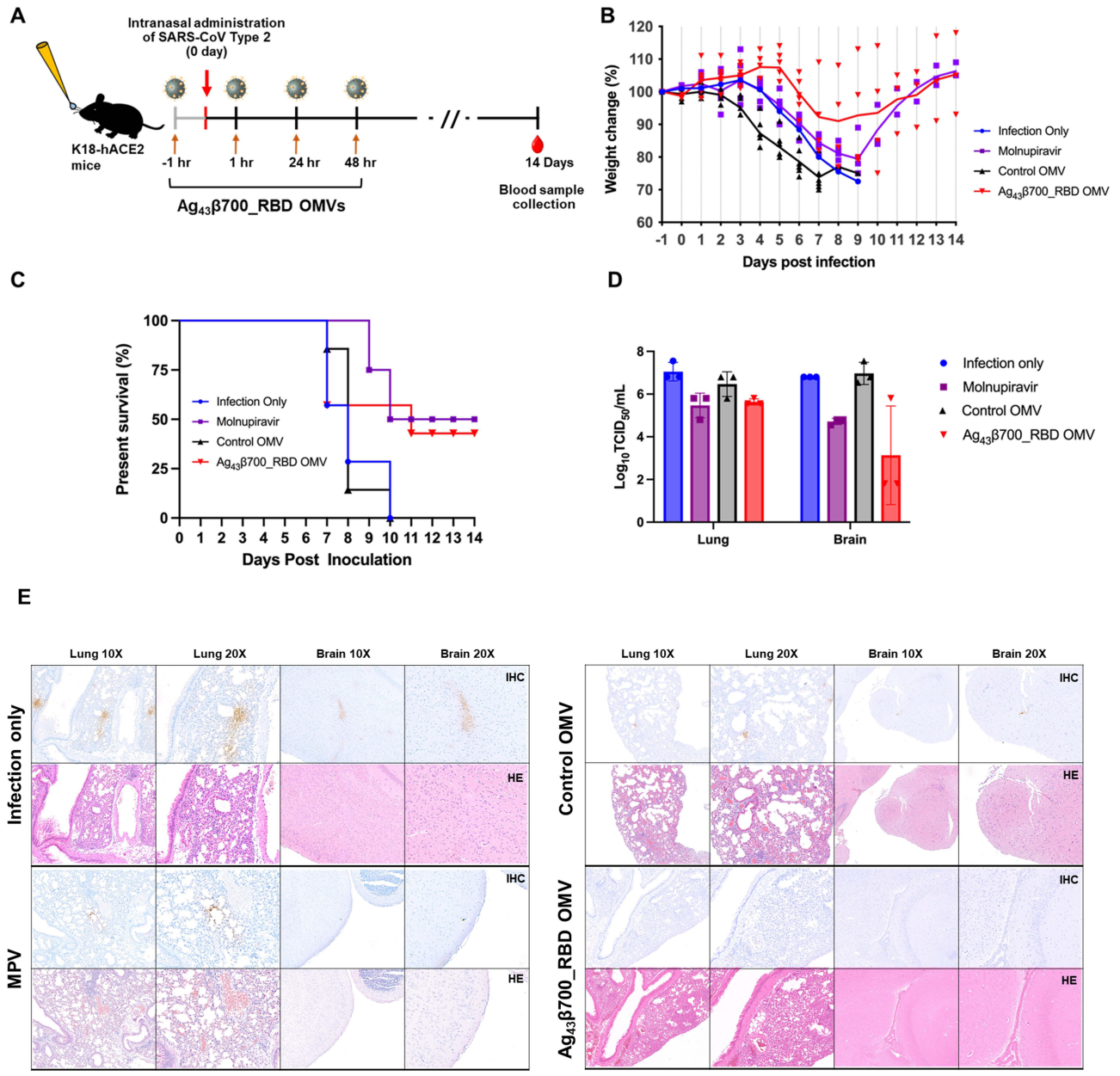

Figure 5 Protection of hACE2 mice against SARS-CoV-2 challenge following intranasal Ag43β700_RBD OMV administration. (**A**) Schematic representation of the immunisation schedule. K18-hACE2 mice (n = 5/group) were intranasally immunised 1 day prior to infection with SARS-CoV-2. Three booster doses were then administered at 1, 24, and 48 h post infection. (**B**) Weight change (%). (**C**) Survival percentage (%). (**D**) Analysis of the viral titres in the lung and brain tissues. Immunisation with Ag43β700_RBD OMVs decreased the viral titre in the SARS-CoV-2-infected mice. (**E**) Histological evaluation of lung and brain sections from K18-hACE2 mice following intranasal infection with 5 MLD50 SARS-CoV-2 5 days post-infection.

Intranasal Immunisation with Ag43β700_RBD OMVs

The complexity of SARS-CoV-2 pathogenesis necessitates multidisciplinary approaches for combating SARS-CoV-2 infection. Currently, there are numerous different therapeutic approaches available, such as cell-based drug delivery therapies, monoclonal antibody/plasma-mediated immunotherapies, and vaccine therapeutics. Recent studies have indicated that intranasal vaccination effectively induces mucosal immunity and prevents mucosal pathogen invasion.[40] We evaluated the efficacy of Ag43β700_RBD OMVs for intranasal immunisation against SARS-CoV-2 (Figure 5A) and found that infected mice lost weight from 4 to 9 DPI (Figure 5B). Mice immunised with Ag43β700_RBD OMVs showed less than 5% weight loss 1 day after administration and then exhibited significant weight loss protection at 9 DPI. It shows a nearly similar recovery rate compared to MPV (positive control), which has been approved by the FDA as a COVID-19 treatment.[41] Whereas there was no

https://doi.org/10.2147/IJN.S497742

significant protection from weight loss in the infection-only and control OMV-treated mice (Figure 5B). Furthermore, mice immunised with Ag43β700_RBD OMVs began to recover their body weight from 8 DPI, whereas mice treated with MPV only began to recover their body weight from 9 DPI. Ag43β700_RBD OMV-immunised mice therefore exhibited greater recovery than MPV-treated mice. Mice immunised with Ag43β700_RBD OMVs exhibited 43% survival (Figure 5C). All tested mice were sacrificed at 5 DPI and, as SARS-CoV-2 mainly replicates in the lung and brain of K18-hACE2 mice,[42,43] these tissues were harvested for viral titre analyses. Compared with the viral titres in the lung tissues of the infection-only group, the viral titres in the lung tissues of both the MPV-treated and the Ag43β700_RBD OMV-immunised groups were reduced to a similar level (Figure 5D). In contrast to the lung tissues, the brain tissue of the Ag43β700_RBD OMV-immunised group showed a 10-fold greater decrease in viral titre than that of the MPV-treated group (Figure 5D). As brain-related abnormalities, such as pathological changes and brain fog, due to SARS-CoV-2 infection are continuously being reported,[44,45] Ag43β700_RBD OMVs may reduce the pathological effects of SARS-CoV-2 in the brain.

To evaluate the antiviral efficacy of Ag43β700_RBD OMV-immunisation, we performed H&E staining and immunohistochemistry on the lung and brain tissues harvested at 5 DPI. Similar to naïve tissue, the lung and brain tissues obtained from Ag43β700_RBD OMV-immunised mice exhibited less severe lesions and reduced inflammation (Figure 5E). Furthermore, immunohistochemical staining for SARS-CoV-2 revealed reduced staining in the lung and brain tissues of Ag43β700_RBD OMV-immunised mice (Figure 5E). These results suggest that intranasal Ag43β700_RBD OMV immunisation has the potential to prevent viral infection.

Discussion

Delivery platform technology for vaccine design to treat infectious diseases has become a crucial tool for enhancing the stability of biomolecules, depending on the lipid composition and ratio. Various delivery systems including lipid nanoparticles, liposomes, and EVs are ongoing to improve the delivery efficacy of biomolecules and minimize potential side effects.[46] Among these, OMVs have also been used as a notable material for vaccine delivery platforms.[47,48] Intrinsic properties of OMVs that encapsulate many biomolecules (*eg* RNA, protein, metabolite) have been well demonstrated. Moreover, they are natural materials, and side effects are significantly lower than synthetic particles. Naturally released OMVs (nOMVs) contain various immunological substances including pathogen-associated molecular patterns (PAMPs), and they are highly attractive as vaccine materials due to their ability to induce immediate innate immune responses.[9] The representative OMV vaccine, BEXSERO, is currently used for *Neisseria meningitidis* (*N. meningitidis*) serogroup B in many countries, and various pharmaceutical companies have been developing new vaccines by leveraging the advantages of OMVs.[10]

Spontaneously released OMVs have low yields, hindering their use for industrial purposes. To overcome this, the development of generalized modules for membrane antigen (GMMA) or mimetic OMVs through chemical treatment methods is commonly employed. In this regard, detergent-based OMVs (dOMVs) production achieves over 10^7 times greater efficiency compared to nOMVs,[16] and it also reduces OMV endotoxicity.

Unlike bacteria, viruses evolve through rapid mutations, leading to the emergence of various variants. To respond to these variants, fast and accurate vaccine development technologies are needed. The most straightforward approach is to develop a modified vaccine tailored to the variant's mutant site like an mRNA vaccine.[49] Our platform is designed with a restriction enzyme site positioned between the signal peptide and the β-barrel sequence. By simply inserting the mutated sequence, the system can be effortlessly reconfigured into a target-specific construct, streamlining the display process. This design facilitates rapid and precise responses to diverse variants and can also be applied to other viral species, such as Dengue, Zika, and Influenza.

In addition to the various advantages mentioned earlier for vaccine applications, it can also be used as a diagnostic tool particularly for neutralizing antibodies (nAbs) diagnosis. Following viral infection or vaccination, the body produces nAbs, which target a structural component of the virus to mitigate or block viral infectivity.[50] Effective defence against viral infection requires enough nAbs. Detection of nAbs allows evaluation of vaccine efficacy,[51] serological diagnosis,[52] and epidemiological investigation.[53] Currently, the plaque-reduction neutralisation test (PRNT) is the most widely used virus neutralisation test (VNT) to measure nAbs. However, PRNTs are complex and require large serum samples and long culture times for plaque formation.[54] Various other methods, such as pseudovirus neutralisation tests (pVNTs) and

Table 2 Comparison with Ag43β700_RBD and Other SARS-CoV-2 Approach Strategy

OMV Source	OMV Isolation	Category	Design	OMV Test		Ref
				Amount	Efficacy	
N. meningitidis	Ultrafiltration	Inactivated virus	Mesoporous silica (SBa15 and SBa16), SARS-CoV-2 and the OMV complex	$5X10^6$ particles/mL of OMV	The range of 0.8 to 1.2 at OD_{490} in the ELISA test for IgG detection	[57]
N. meningitidis	/	RBD protein	Recombinant RBD expressed in CHO cells, OMV and alum complex	10 μg of RBD dimer and 4 ug of OMV	Over 90% inhibition of RBD-ACE2 binding	[47]
S. typhimurium	Ultracentrifugation	RBD protein	Recombinant RBD::Spytag and surface expressed SpyCatcher OMV	$3X10^{10}$ particles of OMV per dose	≦10 of endpoint titer (log2)	[5]
E. coli	Ultrafiltration	RBD-OMV	Bacterial ompA::RBD engineering	10 μg of OMV	2.2 times the antibody titer compared to the control	[58]
E. coli, ClearColi	Lysozyme-based chemical treatment	RBD-OMV	Ag43::RBD autotransporter surface display	8.0×10^8 particles of OMV/mouse	39–58% neutralisation	Our study

Notes: *N. meningitidis: Neisseria meningitidis; S. typhimurium: Salmonella typhimurium; E. coli: Escherichia coli*; ClearColi: LPS free *E. coli.*

surrogate virus neutralisation tests (sVNTs), are also used.[55,56] In our data, Figure 2C and D demonstrate that Ag43β700_RBD OMVs can be applied as a diagnostic material for evaluating neutralizing antibody activity.

Similar studies using OMVs against SARS-CoV-2 are summarized in Table 2. OMVs extracted from various bacteria have been explored as vaccine candidates against SARS-CoV-2 through multiple approaches, including i) inactivated viruses with OMVs, ii) recombinant RBD proteins with OMVs, and iii) one-step synthesis recombinant RBD-OMVs. However, our research is a multi-platform capable of both diagnosis and treatment for COVID-19. The findings suggest that it can serve as an antigen, a platform for neutralizing antibody diagnostics, and an intranasal vaccine material.

Although this study provides theranostic observations, future directions remain. This study was conducted using the small RBD protein (aa 331–524 in Figure 1A), indicating the need for further investigation to apply larger proteins. Additionally, exploring the OMV loading of foreign targets (eg drugs, antigens, mRNA, etc.) is needed to enhance the multivalent approach. Lastly, to understand whether our viral mimetic OMVs can also neutralize other coronaviruses, additional in vitro and in vivo studies will be needed to determine the binding specificity and affinity of circulating variants of concern (VOCs).[18]

This study represents the first case of Ag43β700_RBD OMVs in theranostic approaches against SARS-CoV-2, which may have great potential for synergistic antiviral performance as diagnostic and intranasal vaccine candidates.

Conclusion

Mitigation of virus infections requires rapid, accurate diagnostic methods, as well as therapeutics for disrupting spike protein–host interactions. This study demonstrated the potential of Ag43β700 OMVs in a theranostic approach for SARS-CoV-2 diagnosis and therapy. We demonstrated the diagnostic performance of Ag43β700_RBD OMVs. Furthermore, we found that intranasal immunisation with Ag43β700_RBD OMVs provides strong protection against SARS-CoV-2 by inducing a robust immune response, as well as a detectable level of neutralising antibody against the SARS-CoV-2 RBD. In this study, we focused on the SARS-CoV-2, further investigations are required to cross-validation with other variants or viruses. In conclusion, Ag43β700_RBD OMVs may be applied as a multifaceted theranostic platform for further emerging infectious diseases.

Abbreviations

Ag43, Antigen 43; Ag43β, Ag43 β-barrel; ACE2, Angiotensin-Converting Enzyme 2; AC, Autochaperone; AT, Autotransporter; COVID-19, Coronavirus Disease-2019; dOMVs, Detergent-Based OMVs; hACE2, Human Angiotensin-Converting Enzyme 2; IL, Interleukin; LF, Lateral Flow; LPS, Lipopolysaccharide; MLD_{50}, Mouse Lethal Dose 50; OM, Outer Membrane; OMVs, Outer Membrane Vesicles; nOMVs, Naturally Released OMVs; nAbs, Neutralizing Antibodies; PRNT, Plaque-Reduction Neutralisation Test; pVNTs, Pseudovirus Neutralisation Tests; RBD, Receptor-Binding Protein; SARS-CoV-2, Severe Acute Respiratory Syndrome Coronavirus Type 2; SP, Signal Peptide; SPR, Surface Plasmon Resonance; sVNTs, Surrogate Virus Neutralisation Tests; TNFα, Tumor Necrosis Factor Alpha; UC, Ultracentrifugation; VNT, Virus Neutralisation Test.

Author Contributions

All authors made a significant contribution to the work reported, whether that is in the conception, study design, execution, acquisition of data, analysis and interpretation, or in all these areas; took part in drafting, revising or critically reviewing the article; gave final approval of the version to be published; have agreed on the journal to which the article has been submitted; and agree to be accountable for all aspects of the work.

Funding

This work was supported by a Basic Science Research Program through the National Research Foundation of Korea (NRF) funded by the Ministry of Education (2020R1A6A1A06046235); the National Research Foundation of Korea (NRF) grant funded by the Korea government (MSIT) (RS-2024-00351584); Chungbuk National University in 2023.

Disclosure

The authors declare that they have no competing interests in this work.

References

1. Schwechheimer C, Kuehn MJ. Outer-membrane vesicles from Gram-negative bacteria: biogenesis and functions. *Nat Rev Microbiol*. 2015;13(10):605–619. doi:10.1038/nrmicro3525
2. Petousis-Harris H, Radcliff FJ, Exploitation of Neisseria meningitidis Group B OMV Vaccines Against N. gonorrhoeae to inform the development and deployment of effective gonorrhea vaccines. *Front Immunol*. 2019;10:683. doi:10.3389/fimmu.2019.00683.
3. Gujrati V, Kim S, Kim SH, et al. Bioengineered Bacterial Outer Membrane Vesicles as Cell-Specific Drug-Delivery Vehicles for Cancer Therapy. *Acs Nano*. 2014;8(2):1525–1537. doi:10.1021/nn405724x
4. Brown L, Wolf JM, Prados-Rosales R, Casadevall A. Through the wall: extracellular vesicles in Gram-positive bacteria, mycobacteria and fungi. *Nat Rev Microbiol*. 2015;13(10):620–630. doi:10.1038/nrmicro3480
5. Jiang L, Driedonks TAP, Jong WSP, et al. A bacterial extracellular vesicle-based intranasal vaccine against SARS-CoV-2 protects against disease and elicits neutralizing antibodies to wild-type and Delta variants. *J Extracell Vesicles*. 2022;11(3):e12192. doi:10.1002/jev2.12192
6. Xue KK, Wang L, Liu JY. Bacterial outer membrane vesicles and their functionalization as vehicles for bioimaging, diagnosis and therapy. *Mater Adv*. 2022;3(19):7185–7197. doi:10.1039/d2ma00420h
7. Wan SS, Song GZ, Hu H, et al. Intestine epithelial cell-derived extracellular vesicles alleviate inflammation induced by TcdB through the activity of TGF-β1. *Mol Cell Toxicol*. 2023;19(3):509–519. [doi:ARTN s13273-022-00280-8]. doi:10.1007/s13273-022-00280-8
8. Lee S, Han BK, Kim YH, Ahn JY. SpyCatcher-SpyTagged ApxIA toxoid and the immune-modulating yeast ghost shells. *J Biomed Nanotechnol*. 2020;16(11):1644–1657. doi:10.1166/jbn.2020.2992
9. Weyant KB, Oloyede A, Pal S, et al. A modular vaccine platform enabled by decoration of bacterial outer membrane vesicles with biotinylated antigens. *Nat Commun*. 2023;14(1):464. doi:10.1038/s41467-023-36101-2
10. Micoli F, Adamo R, Nakakana U. Outer membrane vesicle vaccine platforms. *BioDrugs*. 2024;38(1):47–59. doi:10.1007/s40259-023-00627-0
11. Ramesh B, Sendra VG, Cirino PC, Varadarajan N. Single-cell characterization of autotransporter-mediated Escherichia coli surface display of disulfide bond-containing proteins. *J Biol Chem*. 2012;287(46):38580–38589. doi:10.1074/jbc.M112.388199
12. Choi HJ, Ahn G, Yu US, Kim EJ, Ahn JY, Chan Jeong O. Pneumatically driven microfluidic platform and fully automated particle concentration system for the capture and enrichment of pathogens. *ACS Omega*. 2023;8(31):28344–28354. doi:10.1021/acsomega.3c02264
13. Henderson IR, Navarro-Garcia F, Desvaux M, Fernandez RC, Ala'Aldeen D. Type V protein secretion pathway: the autotransporter story. *Microbiol Mol Biol Rev*. 2004;68(4):692–744. doi:10.1128/MMBR.68.4.692-744.2004
14. Heras B, Totsika M, Peters KM, et al. The antigen 43 structure reveals a molecular Velcro-like mechanism of autotransporter-mediated bacterial clumping. *Proc Natl Acad Sci U S A*. 2014;111(1):457–462. doi:10.1073/pnas.1311592111
15. Jing KJ, Guo YL, Ng IS. Antigen-43-mediated surface display revealed in by different fusion sites and proteins. *Bioresour Bioprocess*. 2019;6(1):ARTN14. doi:10.1186/s40643-019-0248-6
16. Ahn G, Yoon HW, Choi JW, et al. Structural stability for surface display of antigen 43 and application to bacterial outer membrane vesicles production. *BMB Rep*. 2024;57(8):369–374. doi:10.5483/BMBRep.2024-0056

17. WHO. Statement on the fifteenth meeting of the IHR (2005) Emergency Committee on the COVID-19 pandemic. Available from: https://www.who.int/news/item/05-05-2023-statement-on-The-fifteenth-meeting-of-The-international-health-regulations-(2005)-emergency-committee-regarding-The-coronavirus-disease-(covid-19)-pandemic. Accessed May 4, 2023.
18. WHO COVID-19 dashboard. Number of COVID-19 cases reported to WHO. Available from: https://covid19.who.int/. Accessed December 22, 2024.
19. Huang Y, Yang C, Xu XF, Xu W, Liu SW. Structural and functional properties of SARS-CoV-2 spike protein: potential antivirus drug development for COVID-19. *Acta Pharmacol Sin*. 2020;41(9):1141–1149. doi:10.1038/s41401-020-0485-4
20. Lan J, Ge J, Yu J, et al. Structure of the SARS-CoV-2 spike receptor-binding domain bound to the ACE2 receptor. *Nature*. 2020;581:7807):215–220. doi:10.1038/s41586-020-2180-5
21. Saraswat I, Saha S, Mishra A. A review of metallic nanostructures against severe acute respiratory syndrome coronavirus 2 (SARS-CoV-2). *Toxicol Env Health*. 2023;15(4):315–324. doi:10.1007/s13530-023-00182-9
22. Park M, Yoo G, Bong J-H, Jose J, Kang M-J, Pyun J-C. Isolation and characterization of the outer membrane of Escherichia coli with autodisplayed Z-domains. *Biochimica et Biophysica Acta (BBA)-Biomembranes*. 2015;1848(3):842–847. doi:10.1016/j.bbamem.2014.12.011
23. Song HW, Yoo G, Bong JH, Kang MJ, Lee SS, Pyun JC. Surface display of sialyltransferase on the outer membrane of Escherichia coli and ClearColi. *Enzyme Microb Technol*. 2019;128:1–8. doi:10.1016/j.enzmictec.2019.04.017
24. Sekhon SS, Shin WR, Kim SY, et al. Cyclophilin A-mediated mitigation of coronavirus SARS-CoV-2. *Bioeng Transl Med*. 2022;8(2):e10436. doi:10.1002/btm2.10436
25. Yi CY, Sun XY, Ye J, et al. Key residues of the receptor binding motif in the spike protein of SARS-CoV-2 that interact with ACE2 and neutralizing antibodies. *Cell. Mol. Immunol.* 2020;17(6):621–630. doi:10.1038/s41423-020-0458-z
26. Han PC, Su C, Zhang YF, et al. Molecular insights into receptor binding of recent emerging SARS-CoV-2 variants. *Nat Commun*. 2021;12(1):ARTN6103. doi:10.1038/s41467-021-26401-w
27. Barton MI, MacGowan SA, Kutuzov MA, Dushek O, Barton GJ, van der Merwe PA. Effects of common mutations in the SARS-CoV-2 Spike RBD and its ligand, the human ACE2 receptor on binding affinity and kinetics. *Elife*. 2021;10. doi:10.7554/eLife.70658
28. Hu K, Palmieri E, Samnuan K, et al. Generalized Modules for Membrane Antigens (GMMA), an outer membrane vesicle-based vaccine platform, for efficient viral antigen delivery. *J Extracell Vesicles*. 2022;11(11):e12247. doi:10.1002/jev2.12247
29. Zhang M, Wang L, Liu J, Pang Y. Envelope virus-mimetic nanovaccines by hybridizing bioengineered cell membranes with bacterial vesicles. *Iscience*. 2022;25(6):104490. doi:10.1016/j.isci.2022.104490
30. Zhang L, Zhang Y, Qin X, et al. Recombinant ACE2 protein protects against acute lung injury induced by SARS-CoV-2 spike RBD protein. *Crit Care*. 2022;26(1):171. doi:10.1186/s13054-022-04034-9
31. Shang J, Wan Y, Luo C, et al. Cell entry mechanisms of SARS-CoV-2. *Proc Natl Acad Sci U S A*. 2020;117(21):11727–11734. doi:10.1073/pnas.2003138117
32. Suhail S, Zajac J, Fossum C, et al. Role of Oxidative Stress on SARS-CoV (SARS) and SARS-CoV-2 (COVID-19) Infection: a Review. *Protein J*. 2020;39(6):644–656. doi:10.1007/s10930-020-09935-8
33. Mehdipour AR, Hummer G. Dual nature of human ACE2 glycosylation in binding to SARS-CoV-2 spike. *Proc Natl Acad Sci U S A*. 2021;118(19). doi:10.1073/pnas.2100425118
34. Allen JD, Watanabe Y, Chawla H, Newby ML, Crispin M. Subtle Influence of ACE2 glycan processing on SARS-CoV-2 recognition. *J Mol Biol*. 2021;433(4):166762. doi:10.1016/j.jmb.2020.166762
35. Mamat U, Woodard R, Wilke K, et al. Endotoxin-free protein production—ClearColi™ technology. *Nat Methods*. 2013;10(9):916. doi:10.1038/nmeth.f.367
36. Cao H, Mai J, Zhou Z, et al. Intranasal HD-Ad vaccine protects the upper and lower respiratory tracts of hACE2 mice against SARS-CoV-2. *Cell Biosci*. 2021;11(1):202. doi:10.1186/s13578-021-00723-0
37. Rothen D, Krenger P, Nonic A, et al. Intranasal administration of a VLP-based vaccine induces neutralizing antibodies against SARS-CoV-2 and variants of concern. *Swiss Med Weekly*. 2022;152:14s.
38. Ganesan S, Acosta H, Brigolin C, et al. Intranasal nanoemulsion adjuvanted S-2P vaccine demonstrates protection in hamsters and induces systemic, cell-mediated and mucosal immunity in mice. *PLoS One*. 2022;17(11):e0272594. doi:10.1371/journal.pone.0272594
39. Stark FC, Akache B, Deschatelets L, et al. Intranasal immunization with a proteosome-adjuvanted SARS-CoV-2 spike protein-based vaccine is immunogenic and efficacious in mice and hamsters. *Sci Rep*. 2022;12(1):ARTN9772. doi:10.1038/s41598-022-13819-5
40. Alu A, Chen L, Lei H, Wei Y, Tian X, Wei X. Intranasal COVID-19 vaccines: from bench to bed. *EBioMedicine*. 2022;76:103841. doi:10.1016/j.ebiom.2022.103841
41. Jayk Bernal A, Gomes da Silva MM, Musungaie DB, et al. Molnupiravir for oral treatment of covid-19 in nonhospitalized patients. *N Engl J Med*. 2022;386(6):509–520. doi:10.1056/NEJMoa2116044
42. Winkler ES, Bailey AL, Kafai NM, et al. SARS-CoV-2 infection of human ACE2-transgenic mice causes severe lung inflammation and impaired function. *Nat Immunol*. 2020;21(11):1327–1335. doi:10.1038/s41590-020-0778-2
43. Seehusen F, Clark JJ, Sharma P, et al. Neuroinvasion and Neurotropism by SARS-CoV-2 Variants in the K18-hACE2 Mouse. *Viruses*. 2022;14(5). doi:10.3390/v14051020
44. Ding Q, Zhao H. Long-term effects of SARS-CoV-2 infection on human brain and memory. *Cell Death Discov*. 2023;9(1):196. doi:10.1038/s41420-023-01512-z
45. Fernández-Castañeda A, Lu PW, Geraghty AC, et al. Mild respiratory COVID can cause multi-lineage neural cell and myelin dysregulation. *Cell*. 2022;185(14):2452–+. doi:10.1016/j.cell.2022.06.008
46. Marquez CA, Oh CI, Ahn G, Shin WR, Kim YH, Ahn JY. Synergistic vesicle-vector systems for targeted delivery. *J Nanobiotechnology*. 2024;22(1):6. doi:10.1186/s12951-023-02275-6
47. Santana-Mederos D, Perez-Nicado R, Climent Y, et al. A COVID-19 vaccine candidate composed of the SARS-CoV-2 RBD dimer and Neisseria meningitidis outer membrane vesicles. *RSC Chem Biol*. 2022;3(2):242–249. doi:10.1039/d1cb00200g
48. Park KS, Svennerholm K, Crescitelli R, et al. Detoxified synthetic bacterial membrane vesicles as a vaccine platform against bacteria and SARS-CoV-2. *J Nanobiotechnol*. 2023;21(1):ARTN.156. doi:10.1186/s12951-023-01928-w

49. Mir S, Mir M. The mRNA vaccine, a swift warhead against a moving infectious disease target. *Expert Rev Vaccines*. 2024;23(1):336–348. doi:10.1080/14760584.2024.2320327
50. Li D, Sempowski GD, Saunders KO, Acharya P, Haynes BF. SARS-CoV-2 Neutralizing Antibodies for COVID-19 prevention and treatment. *Annu Rev Med*. 2022;73(1):1–16. doi:10.1146/annurev-med-042420-113838
51. Follmann D, O'Brien MP, Fintzi J, et al. Examining protective effects of SARS-CoV-2 neutralizing antibodies after vaccination or monoclonal antibody administration. *Nat Commun*. 2023;14(1):3605. doi:10.1038/s41467-023-39292-w
52. Muruato AE, Fontes-Garfias CR, Ren P, et al. A high-throughput neutralizing antibody assay for COVID-19 diagnosis and vaccine evaluation. *Nat Commun*. 2020;11(1):4059. doi:10.1038/s41467-020-17892-0
53. Tani H, Inasaki N, Yazawa S, et al. Neutralizing antibody levels and epidemiological characteristics of patients with breakthrough COVID-19 infection in Toyama, Japan. *Jpn J Infect Dis*. 2023;76(5):319–322. doi:10.7883/yoken.JJID.2023.100
54. Bewley KR, Coombes NS, Gagnon L, et al. Quantification of SARS-CoV-2 neutralizing antibody by wild-type plaque reduction neutralization, microneutralization and pseudotyped virus neutralization assays. *Nat Protoc*. 2021;16(6):3114–3140. doi:10.1038/s41596-021-00536-y
55. Huang Y, Borisov O, Kee JJ, et al. Calibration of two validated SARS-CoV-2 pseudovirus neutralization assays for COVID-19 vaccine evaluation. *Sci Rep*. 2021;11(1):23921. doi:10.1038/s41598-021-03154-6
56. Tan CW, Chia WN, Qin X, et al. A SARS-CoV-2 surrogate virus neutralization test based on antibody-mediated blockage of ACE2–spike protein–protein interaction. *Nat Biotechnol*. 2020;38(9):1073–1078. doi:10.1038/s41587-020-0631-z
57. Bernardes BG, Moura AD, Guarnieri JPO, et al. Vaccination with outer membrane vesicles from Neisseria Meningitidis and SBa15, SBa16 mesoporous silica associated with SARS-CoV-2 induces protective humoral and cellular response against COVID-19 in mice. *Braz J Infect Dis*. 2024;28(6):104479. doi:10.1016/j.bjid.2024.104479
58. Wo J, Lv ZY, Sun JN, Tang H, Qi N, Ye BC. Engineering probiotic-derived outer membrane vesicles as functional vaccine carriers to enhance immunity against SARS-CoV-2. *Iscience*. 2023;26(1):ARTN105772. doi:10.1016/j.isci.2022.105772